


## RESEARCH ARTICLE

# Antibacterial activities of centrifugally spun polyethylene oxide/silver composite nanofibers

Md Toukir Hasan<sup>1</sup> | Ramiro Gonzalez<sup>1</sup> | Mircea Chipara<sup>2</sup> | Luis Materon<sup>3</sup> | Jason Parsons<sup>4</sup> | Mataz Alcoutlabi<sup>1</sup> 

<sup>1</sup>Mechanical Engineering Department, University of Texas Rio Grande Valley, Edinburg, Texas

<sup>2</sup>Physics and Astronomy Department, University of Texas Rio Grande Valley, Edinburg, Texas

<sup>3</sup>Department of Biology, University of Texas Rio Grande Valley, Edinburg, Texas

<sup>4</sup>Department of Chemistry, University of Texas Rio Grande Valley, Edinburg, Texas

## Correspondence

Mataz Alcoutlabi, Mechanical Engineering Department, University of Texas Rio Grande Valley, Edinburg, Texas, USA.  
Email: mataz.alcoutlabi@utrgv.edu

## Abstract

Composite nanofibers were prepared successfully by centrifugal spinning of poly(ethylene oxide) aqueous solutions containing silver nanoparticles. The core focus of the present work is to carefully evaluate the antibacterial activity of poly(ethylene oxide)-Ag composite nanofibers in the presence of *Escherichia coli* (*E. coli*) and *Bacillus cereus* (*B. cereus*) bacteria. Centrifugally spun nanofibers were obtained from poly(ethylene oxide)-Ag precursor solutions with different Ag nanoparticle loadings. The process parameters such as the spinneret rotational speed, collector-spinneret distance, and relative humidity were optimized to obtain fine fibers. The complex morphology and flexible structure of the poly(ethylene oxide)-Ag composite fibers were investigated by scanning electron microscopy, X-ray diffraction, energy-dispersive X-ray spectroscopy, thermogravimetric analysis, and Raman spectroscopy. The composite nanofibers have been proven as a strong antibacterial agent against *E. coli* and *B. cereus* due to their capacity to form superior inhibition zones. The efficiency of inhibiting bacteria by nanofibers was over 98%. The workability of the bacteria was impeded by the nanofibrous membrane as the Ag nanoparticles presented an effective chemical ability to dysfunction the bacterial structure at the nanoscale. These results demonstrate that the centrifugally spun poly(ethylene oxide)-Ag nanofibers are promising antibacterial agents for biomedical applications.

## KEYWORDS

antibacterial activity, centrifugal spinning, polyethylene oxide, silver nanoparticles

## 1 | INTRODUCTION

Bacterial pitfalls are harmful to our health and commercial products. A typical resident of human intestine, Gram-negative *E. coli* bacteria, causes nosocomial infections in the urinary areas.<sup>1,2</sup> Conversely, Gram-positive bacteria, *B. cereus* makes deep penetration of attack into human body.<sup>3</sup> To overcome these problems, polymer/metal nanocomposites have recently been used as antimicrobial scaffolds for cell adhesion and proliferation<sup>4</sup> due to their biocompatibility, availability, and biodegradability.<sup>5</sup> Since the polymer matrix characteristics

are compatible with the human skin,<sup>6,7</sup> research was focused on absorbing exudates<sup>8-11</sup> as a potential future way to treat infections. The high surface area to volume ratio of nanofibers promotes enhanced porosity. The size, shape, and composition of nanofibers assist the interfacial strength to adjoin the fiber-matrix layers.<sup>12-14</sup>

Nanofibers can be prepared by diverse methods including electrospinning, centrifugal spinning, melt blown spinning, dry spinning, phase separation, template synthesis, and self-assembly.<sup>15</sup> Among all, electrospinning has been the most used method to produce nano- and microfibers in that the conducting polymer solution

jets are drawn to a collector by an electric field.<sup>15,16</sup> Alternatively, centrifugal spinning, a rising promising technique, has been utilized to prepare fibers/microfibers/nanofibers at a moderate cost and at a far higher production rate (1 g/min) than electrospinning (0.3 g/h).<sup>17–20</sup> Additionally, in centrifugal spinning, both conducting and non-conducting solutions/melts can be used to produce the fibers, depending upon the optimized processing parameters.<sup>21–23</sup>

Polyethylene oxide (PEO) is a water-soluble,<sup>24</sup> biodegradable, biocompatible,<sup>5</sup> and chemically stable polymer that can be spun by centrifugal spinning<sup>5</sup> into nano- and microfibers. The combined effect of covalent and hydrogen bonding<sup>25</sup> can contribute to the stability of PEO.<sup>26</sup> Moreover, PEO nanofibers with low toxicity<sup>27</sup> and high surface area to volume ratio are capable to promote the adhesion and growth of organic cells.<sup>28,29</sup> Due to these attractive characteristics, nonwoven PEO fibers have been utilized in various applications such as biomedical,<sup>30</sup> tissue engineering, electronics, energy storage, hemostatic agents,<sup>31</sup> and antibacterial agents.<sup>32</sup>

Most recent studies report that most of the antibacterial agents were developed by electrospinning from natural/synthetic polymer nanocomposite precursors. Monitored antimicrobial activity of electrospun PEO/chitosan/Ag nanofibers, PEO blends–Ag nanoparticles (NPs),<sup>33</sup> as well as PVP/ZnO nanocomposite have demonstrated strong and efficient inhibition against *E. coli* and *S. aureus* bacteria.<sup>34,35</sup> At present, many developed nanofibers are available; however, centrifugally spun PEO nanofibers are exceptionally propitious as a powerful and natural antimicrobial agent against bacteria while having no adverse effects. For instance, PEO hydrogel<sup>32</sup> works quite finely in the digestive tract surgery of antithrombogenic applications.<sup>31</sup> Recently, the efficacy of PEO hydrogels has been testified upon animal bodies as a cured wound.<sup>32,36</sup> Many discovered polymers have no antimicrobial functionality, but such polymers conjugated with other polymers/nanoparticles can display significant properties. Similarly, chitosan, a natural polymer having mediocre antimicrobial function, is extremely difficult to spin. However, chitosan along with PEO can induce high scaffolds to inhibit bacterial infections.<sup>37</sup> Besides, heavy metals can also serve as an antibacterial agent with conjugated polymers. Owing to protonated H<sup>+</sup> ion in chitosan, acidic medium in PEO/chitosan<sup>38</sup> facilitates antimicrobial activities by taking up heavy metals such as Cu, Cd, Mg, and Ag. Therefore, it is confirmed that PEO nanofibers self-autonomously display some antibacterial function, which is amplified by nanoparticles.<sup>33</sup>

Nanofibers prepared from polymer blends and co-polymers may function as a great antimicrobial agent. Avci et al reported results on the use of PVA/PEO with henna extract (2.793 wt%) as a potent eco-friendly agent, which exhibited good outcome against *E. coli* bacteria.<sup>37</sup> Beyond PEO, subsequently, Marini et al<sup>39</sup> introduced a hybrid material as an antibacterial activator based on which Selvam et al,<sup>35</sup> experimentally demonstrated that ZnO NPs (only 20 mg/L)/PVP functionalized with cotton fabric exhibited 100% efficiency to eradicate bacterial spread through a chemical reaction on bacterial surfaces within short time duration. In addition, porous shapes of TiO<sub>2</sub>/Ag nanocomposite ease to agglomerate considerable interactions between particles, which play a major role to impede *E. coli*

and methicillin-resistant *S. aureus* within 24 h.<sup>40–42</sup> Indeed, TiO<sub>2</sub> nanocomposites could not damage the bacterial cell without light and participation of heavy metals (Ag, Cu, Pd).<sup>41–43</sup> Such findings report that despite countless polymers/NPs having antimicrobial capacity, PEO is unique as it is altogether a hydrogel, easy to spin, and, most importantly, an effective activator to recoil Ag NPs through its fibrous matrix.

Many researchers experimented on various NPs to discover the best antibacterial agent where, in the most cases, Ag NPs revealed an outstanding inhibition performance. Shamel et al<sup>42</sup> found that in polyethylene glycol (PEG), Ag NPs can easily be aggregated uniformly along fibrous layers to inhibit *S. aureus* and *Salmonella typhimurium*.<sup>44</sup> Fatma et al<sup>43</sup> reported results in that the inhibition efficiency of PVB/ZnO, PVB/CuO, PVB/ZnO/TiO<sub>2</sub>, and PVB/AgNO<sub>3</sub> was gained 100% within 1–2 h. However, PVB/TiO<sub>2</sub>, PVB/ZrO<sub>2</sub>, and PVB/SnO<sub>2</sub> took more than 4 h to impede bacteria completely. Among above all, PVB/AgNO<sub>3</sub> composite fibers were characterized with the lowest diameter (295 nm) and largest surface porosity (69.5%), assisting Ag to be embedded finely in the fiber's membrane to deteriorate bacterial viability at a limited time.<sup>43</sup> Generally, the inhibition capacity of CS/PEO is only 81.38% and 85.41% against *E. coli* and *S. aureus*, respectively. On the other hand, in conjunction with Ag NPs, CS/PEO displayed 100% inhibition.<sup>34</sup> In fact, PVA/Ag/nanocellulose film worked well against *E. coli* and *S. aureus* since such nanocomposite films exhibited no cytotoxicity effect.<sup>45</sup> Quirós et al<sup>46</sup> analyzed the most effective antibacterial agent with electrospun PVP nanofibers containing Cu, Ag, and Zn nanoparticles. The results indicated that among three of the NPs, Ag NPs exhibited the highest inhibition efficiency (>90%), whereas Zn and Cu showed less antibacterial properties. More importantly, Ag NP is a good capping agent to damage the bacterial cell strains very fast, but Cu and Zn NPs entrapped in PVP nanofibers allow the slow release of dissolved metal to inactivate bacteria. In summary, it has been confirmed that Ag NPs are a strong antibacterial agent (efficiency >99.8%) because of having capacity to disperse and adjoin uniformly into fiber matrixes.<sup>47</sup>

Among all heavy metals, Ag is the highest toxic metal toward microorganism and displays the lowest toxicity for humans.<sup>48</sup> Ag NPs slowly instill into the negatively charged bacteria cell to invade via Ag<sup>+</sup> reacting with (-SH), phosphate groups of bacteria,<sup>49</sup> and generating a leakage on the outer surface. Eventually, Ag<sup>+</sup> sterilizes respiration through continuous reactions with enzymes and proteins of bacterial cells which inactivate bacterial functionality.<sup>50</sup>

The objectives of this work are the processing and characterization of PEO/Ag composite nanofibers and to study their antibacterial activities against *E. coli* and *B. cereus* bacteria. In this study, the use of PEO nanofibers with high surface area to volume ratio as a polymer–fiber matrix for Ag nanoparticle can result in improving their antimicrobial function<sup>51</sup> against common and existing bacteria. The PEO/Ag fibrous membranes can be directly used for wound dress-healing and drug delivery. In addition, the PEO fiber–matrix is biodegradable and biocompatible to human body, whereas using Ag NPs is not practical and difficult to implement in human body as a healing agent. In this

manuscript, a range of Ag NPs concentrations, which are effective to dysfunction microbial attack, is clearly specified.

In this study, PEO/Ag composite nanofibers were prepared by centrifugal spinning of PEO/Ag precursor solutions. The morphology, elemental analysis, thermal dissociation analysis, molecular vibration observation, and crystallographic phase analysis were characterized by SEM, EDS, TGA, RAMAN, and XRD instruments, respectively. The antibacterial activity of PEO/Ag nanocomposite fibers was studied against *E. coli* and *B. cereus* bacteria using agar plate to observe the inhibition zone. To the best of the authors' knowledge, this is the first study to report results on centrifugally spun PEO/Ag composite nanofibers and their use as an antibacterial agent against bacteria.

## 2 | EXPERIMENTAL

### 2.1 | Materials

PEO with average Mw 600,000 was purchased from Sigma-Aldrich (St. Louis, MO); Ag nanoparticles with sizes ranging between 30 and 50 nm were obtained from US Research Nanomaterials, Inc (Huston, TX). Deionized water was used as the solvent. All chemicals were used as received without further purification.

### 2.2 | Preparation of PEO/Ag composite nanofibers

Firstly, PEO was dissolved in water with 8% (w/w) concentration. The solution was homogenized by a vortex, and then Ag NPs, with different concentrations of 15%, 25%, and 35% (w/w) with respect to PEO, were added to the solution. After sonicating the mixture for 1 h, the as-prepared solution was magnetically stirred overnight. The homogeneous PEO/Ag precursor solution was then used to prepare PEO/Ag composite nanofibers by centrifugal spinning using Cyclone L-1000 M (Fiberio Technology Corporation). Prior to centrifugal spinning, the Ag/PEO solution was injected into a spinneret equipped with 30-gauge half-inch regular bevel needles. Sufficient centrifugal forces were applied to the solution to break down the surface tension of the polymer droplets and stretch out the fibers.<sup>52-56</sup> To obtain good fibrous mats, the optimum centrifugal spinning rate and spinneret rotational speed were determined. The centrifugal spinning of PEO/Ag solutions was performed in air at spinneret rotational speeds of 6000 and 8000 rpm and at a relative humidity of 45% ± 5% and at room temperature. The fibers were collected in a well-arranged eight uniform spacious vertical collectors. Finally, the PEO/Ag composite nanofibers were kept in an Al foil and dried for 24 h in a vacuum oven.

### 2.3 | Characterization

The morphology of PEO/Ag composite fibers was characterized by scanning electron microscopy (FE-SEM; Sigma VP Carl Zeiss,

Germany). For high-quality SEM images, the samples were sputtered with a thin layer gold coating using a Denton's Desk V deposition system. From the SEM images with ×5000 magnification, the average fiber diameter was calculated by measuring 130 counts of randomly selected images by using the image analysis software JMicroVision V.1.2.7 (University of Geneva, Geneva, Switzerland) and Origin Pro<sup>®</sup> 2020 software.

Energy dispersive spectroscopy (EDS) (USA) analysis was conducted to evaluate the presence of Ag nanoparticles in the PEO nanofibers. The elemental composition was investigated concisely using samples with various Ag NP content. During the experiments, different areas were focused, and the corresponding peaks were taken into consideration while EDS mapping measurements were taken in the same areas.

Thermogravimetric analysis (TGA) of the samples were studied using TA-Q series equipment, TGAQ500 (TA Instruments Inc.). Samples of about 10 mg were kept in the instrument and heated from 26°C to 700°C at a heating rate of 5°C/min under air atmosphere.

X-ray diffraction (XRD) was performed to visualize the crystalline structure of the nanocomposites. Advance X-ray diffractometer (Bruker, Germany), AXS D8 of graphite monochromator ( $\lambda = 1.5406 \text{ \AA}$ ), was used to characterize the structure of the PEO/Ag composite fibers. The instrument uses CuK alpha as a radiation source. The intensity of the scattered rays and angle ( $2\theta$ ) were measured to investigate the crystal structure of the samples.

In order to investigate the molecular motions within the PEO/Ag composite nanofibers, a Renishaw InVia confocal microscope was used to conduct Raman measurements with 785 (red) and 532 (green) nm excitation laser.

For the characterization of antibacterial performance, PEO/Ag composite nanofibers were tested on the Gram-negative bacteria *E. coli* and Gram-positive bacteria *B. cereus* separately. The antibacterial tests were basically analyzed according to the Kirby Bauer disk diffusion method. Agar plate was setup, and aliquots of 100  $\mu\text{l}$  of a bacterial suspension were spread onto the surface of agar plates uniformly by a sterile L-shape glass rod. The fibrous mats were then carefully deposited on the surface of the agar plates. Eventually, the fibers were incubated at 37°C for 48 h to detect the inhibition zone.

For in vitro release experiments, the Ag NPs were placed in 10 ml of ultrapure water (resistance 18 mOHM) and equilibrated on a nutating mixer. The samples were equilibrated for 24 h, removed, centrifuged at 3000 RPM, and then a 0.5 ml aliquot was taken in triplicate. The samples were then placed back on the nutating mixer and then equilibrated for 48 h and samples. This process of equilibrating for 48 h and sampling was continued for 7 day. The concentration of silver released from the samples was determined using a Perkin Elmer 8300 Optima ICP-OES. The silver concentration was determined using a wavelength of 328.068 nm, a nebulizer flow of 0.65 L/min, a plasma flow of 20 L/min, an auxiliary flow of 0.2 L/min, and an RF power of 1500 W. All samples were collected in triplicate for statistical purposes.

### 3 | RESULTS AND DISCUSSIONS

#### 3.1 | Morphology and structure of fibers

The formation of centrifugally spun fibers depends on the required rotational speed to overcome surface tension of the solution and on the polymer concentration, relative humidity, and the spinneret-to-collector. A control of these parameters is required to produce bead-free and uniform nanofibers. Experimentally, a PEO aqueous solution with 8 wt% concentration produced excellent fibers by centrifugal spinning. Below this concentration, minimal viscosity tended to yield beaded fibers. Moreover, for fine PEO fiber production, the spinneret rotational speed was required to set at 4500 rpm to 8000 rpm at a favorable humidity. However, rotational speeds lower than 4000 rpm barely produced morphologically fine fibers due to the higher surface

tension of the polymer droplets. On the other hand, above 9000 rpm, the centrifugal forces could easily overcome the surface tension and the ejected droplets got enough time to evaporate. Consequently, more jets came out very fast from the spinneret to negatively affect the deposition of fibers on the collector.

As presented in the SEM images of Figure 1, the average fiber diameter ranges from 216 to 244 nm for different concentrations of Ag. The histograms in Figure 1 (C, F, I) show that the average diameter of the PEO/Ag composite nanofibers decreases with increasing the Ag NPs loading in the PEO-fiber matrix which is in agreement with previous experimental results.<sup>57</sup>

The SEM images (Figures 1(A, B, D, E, G, H)) show that the increase of Ag concentration in the PEO solution results in bead-free PEO/Ag composite fibers having fine morphology. It is observed in the SEM images that the Ag NPs tend to agglomerate on the fiber

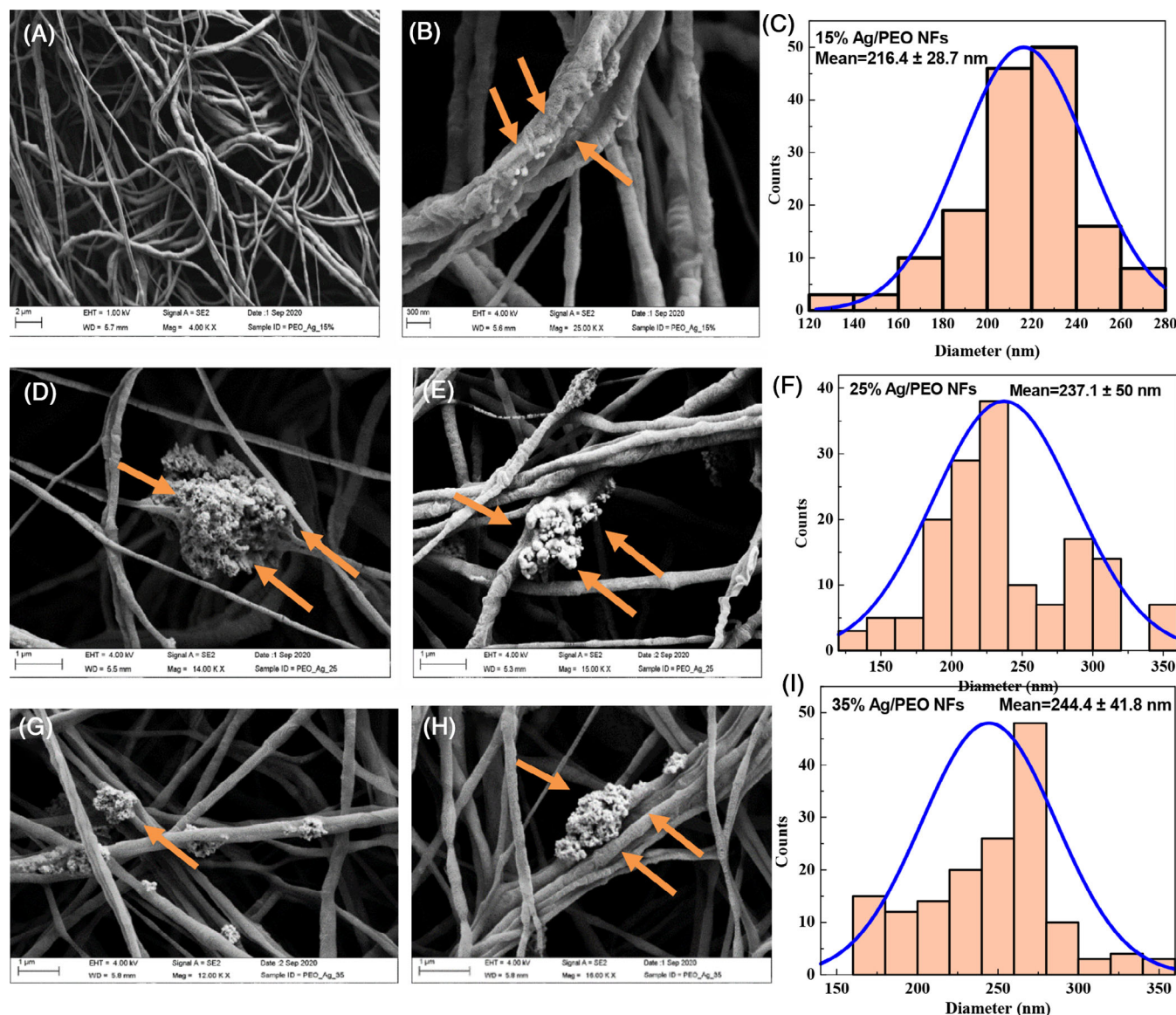


**FIGURE 1** SEM images of the PEO/Ag composite nanofibers with 15, 25, and 35 wt% Ag concentrations in the precursor solution ([A, B], [D, E], [G, H]), respectively. The average fiber diameter distribution (histogram) (C, F, I)

surface. To ensure the presence of Ag NPs in the SEM images, the arrow heads indicate a little bit defected shape of irregularity in the fibrous texture.

Furthermore, the aggregation of Ag NPs in the PEO/Ag composite fibers was caused by the high PEO concentration in the solution. Unlike electrospinning, the centrifugal spinning process requires polymer solutions with high concentration and viscosity where high centrifugal forces are applied to the polymer precursor solution at high rotational speeds to form and stretch the fibers during solvent evaporation. The addition of Ag nanoparticles to the aqueous PEO solution can increase the solution precursor concentration and viscosity further, which can cause more difficulties during centrifugal spinning. Furthermore, the elongation of the polymer jet during the formation of fibers of the precursor solution (polymer/solvent/metallic nanoparticles) can cause a phase separation during spinning.<sup>58,59</sup> Basically, the aggregation of Ag nanoparticles in the PEO-fiber matrix can be mitigated by preparing lower concentration solutions, conducting more sonication at high temperature as well as adding surfactants to the precursor solution. This requires a more in-depth investigation and more work to address this issue.

### 3.2 | Elemental mapping analysis

EDS mapping analysis was conducted using energy dispersive X-ray spectroscopy (EDX) to investigate the elemental composition (especially Ag) in the PEO/Ag composite nanofibers. Figure 2(A–F) shows the EDS mappings with Ag concentrations of 15 wt%. The Ag NPs

(Figure 2(F)) were present in the PEO fibers. The two other elements (C and O) were also detected at higher concentrations than Ag in the selected region. The compositions of the PEO/Ag composite fibers in the EDS-mapping sample area (Figure 2(B)) were 77%, 12%, and 10% of C, O, and Ag, respectively.

It is concluded that the Ag NPs are not embedded within the nanofibers but rather concentrated within defected areas of PEO nanofibers (such as sites where more nanofibers are linked together).

### 3.3 | Thermophysical characterizations

To investigate the thermal degradation of the PEO/Ag composite nanofibers, TGA analysis was performed on the nanofibers under nitrogen atmosphere. The TGA results of the PEO/Ag composite nanofibers with three different Ag concentrations (Figure 3) show similar dependences with important modifications due to the addition of Ag nanoparticles. As the temperature was increased from 25 to 700°C, the mass loss of nanofibers was ignited. The pristine PEO nanofibers are almost volatilized completely at about 550°C, with a low amount of char being noticed (Figure 3(A)). For the PEO/Ag nanocomposites with 25 wt% Ag nanoparticles, the thermal degradation is essentially completed at higher temperatures, with a low amount of residual char, mostly consisting of Ag nanoparticles (Figure 3(A)). There are three main contributions to the mass loss at different temperature. From 25°C to 200°C, the mass loss is very small (Figure 3(A)). This loss represents about 3% weight of the polymer matrix and is caused by water evaporation and formation of

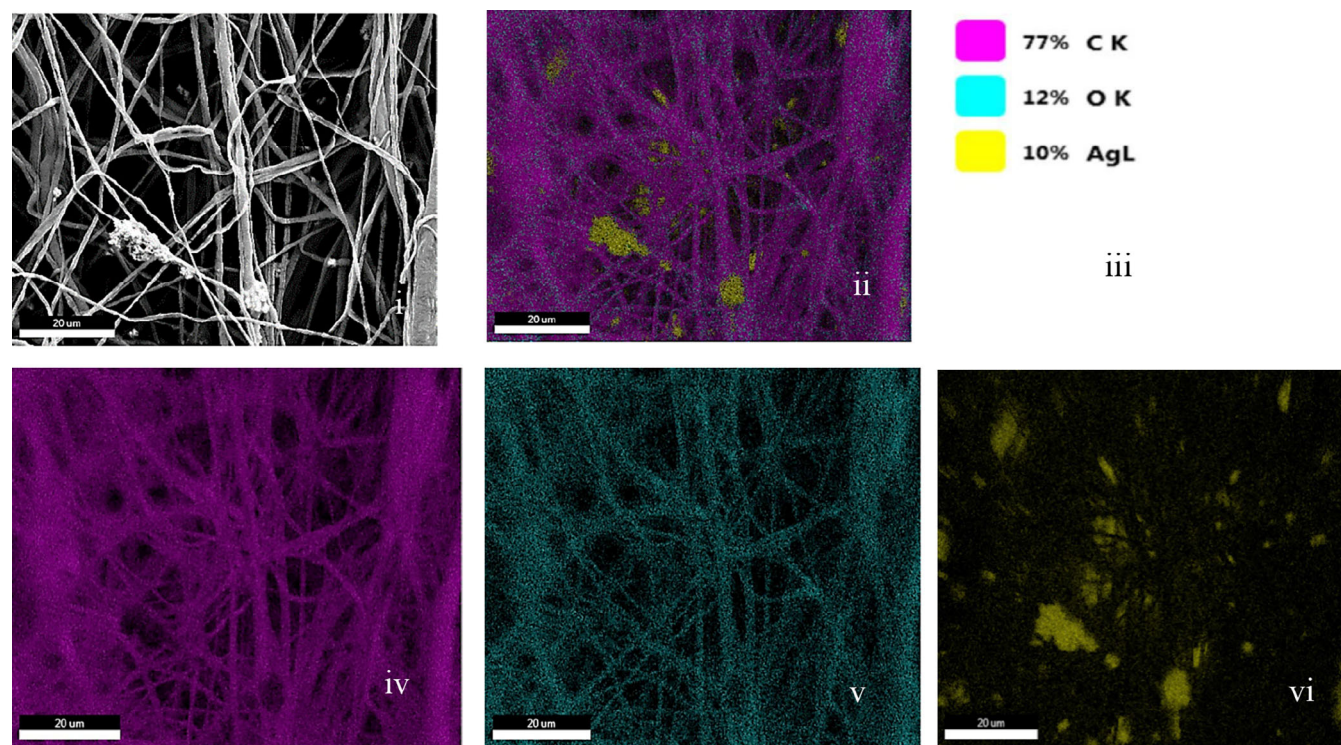


**FIGURE 2** EDS mapping (A) sample area, (B) EDS mapping of PEO/Ag composite fibers, (C) composition of the fibers, (D) C, (E) O, and (F) Ag

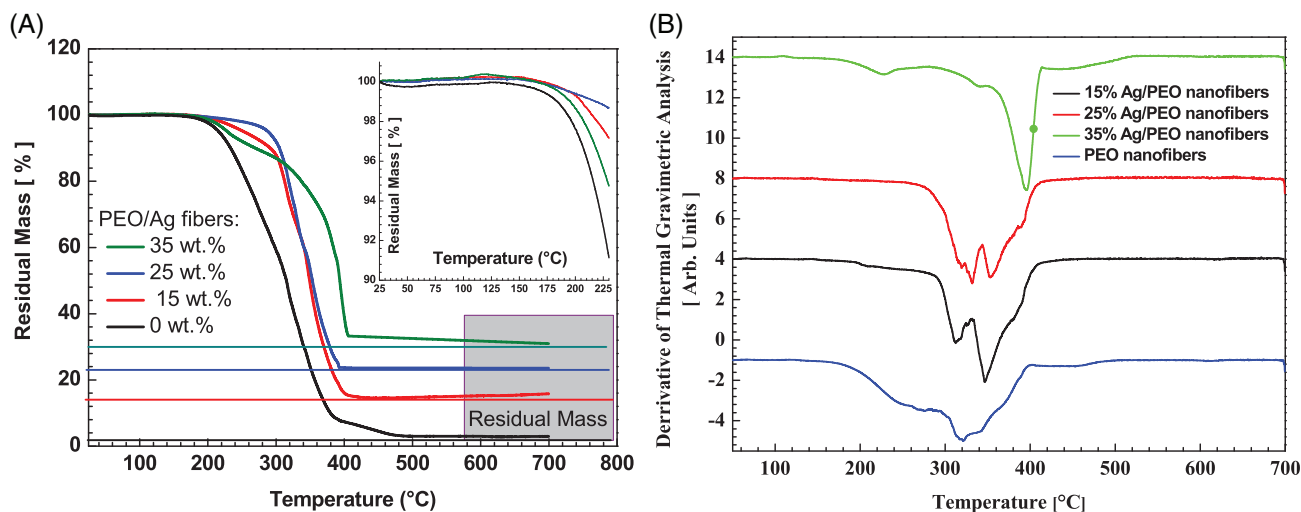


**FIGURE 3** (A) The dependence of the residual mass on temperature for PEO and PEO/Ag composite nanofibers (as recorded by TGA). (B) The dependence of the derivative of the TGA signal on the temperature for PEO and PEO/Ag composite fibers

anhydride. These changes affect the polymer matrix and not the nanofiller. In the second temperature region from 200°C to 400°C, the weight loss of the nanocomposite is substantial and is still controlled by the weight loss occurring within the polymer matrix. At about 700°C, the residual fraction is within the experimental errors which are consistent with the Ag NPs loading in the polymer–fiber matrix.

The thermal degradation at low temperature (below 200°C) is unnoticeable, probably reflecting negligible amounts of water still captured within the nanofibers. The main degradation process is occurring from about 225 to 450°C. In this temperature range, the Ag NPs are essentially shifting the degradation temperature slightly toward higher temperatures. It is observed in Figure 3(A, B) that the weight loss for all samples remains unchanged between 450 and 700°C, indicating that decomposition of the polymer matrix is completed. The residual mass at 700°C is negligible for the pristine PEO nanofibers and consistent, within the experimental errors, with the content of Ag NPs (0 wt%) in the PEO–fiber matrix.

The derivative of the residual mass as a function of temperature (Figure 3(B)) reveals two degradation (negative) peaks in the pristine PEO nanofibers. These peaks are located at a temperature where the mass loss is maximum and eventually suggest two competing degradation mechanisms. The addition of Ag NPs to the PEO fibers narrows these peaks and shifts them slightly to higher temperatures. At about 35 wt% of Ag NPs, there are essentially a single major degradation peak, at about 400°C and some minor broad peaks at lower temperatures.

### 3.4 | XRD analysis

The wide-angle X-ray scattering spectrum of PEO/Ag composite nanofibers is dominated by the peak located at 18.3° in  $2\theta$  assigned to (120) plane reflections (Figure 4). This peak was reported in pristine

PEO at 19.67°,<sup>60</sup> at about 19° in  $2\theta$ ,<sup>61</sup> and even larger  $2\theta$  angles were observed in the case of PEO samples prepared by compression molding.<sup>60</sup>

The observed shift in the (120) peak or line from 19.3° to about 18.3° suggests some interactions between the polymer and the Ag nanoparticles and may include some contributions due to the stretching of the polymer structure during centrifugal spinning. A similar shift (trend) from 19.30° to 19.04° in  $2\theta$  was reported in PEO crystallized on graphene surfaces.<sup>60</sup> The next intense peak was noticed at 22.5°. This peak was typically reported at about 23°,<sup>61</sup> 23.25°,<sup>36</sup> or 23.5°<sup>60</sup> and not properly understood and modeled as it was assigned to several possible reflection planes<sup>62</sup> such as (112).<sup>36</sup> In PEO samples prepared by compression molding, this peak was shifted toward higher  $2\theta$  values<sup>60</sup>; this behavior was assigned to local stresses/strains induced by processing. The as-recorded line (peak) shows an

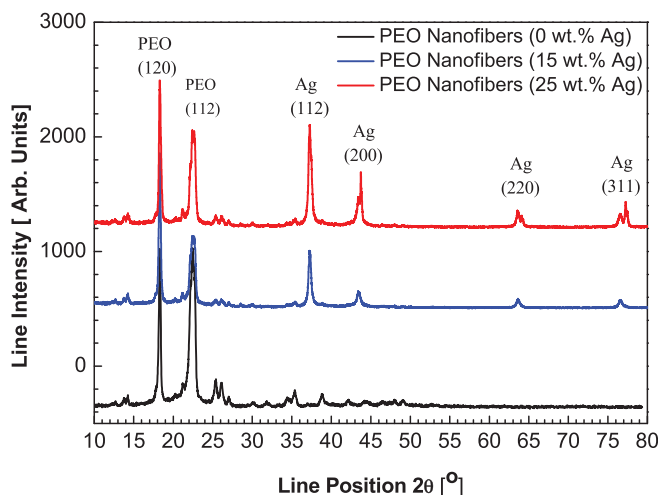


**FIGURE 4** Wide angle X-ray scattering (WAXS) of the pristine PEO and PEO–Ag composite nanofibers

incompletely resolved structure, which may derive for the random orientation of the nanofibers within the mat. The peaks noticed at  $37.3^\circ$  and  $43.9^\circ$  were assigned as (111) and (200) reflections occurring in Ag nanoparticles, respectively, (reported at  $38.18^\circ$  and  $44.25^\circ$  in  $2\theta^{63,64}$ ). The weaker lines originating from Ag nanoparticles and located at  $63.8^\circ$  and  $76.8^\circ$  were assigned to (220) and (311) reflections, respectively, in Ag nanoparticles (reported at  $64.72^\circ$  and  $77.4^\circ$  in Reference 63). The oxidation of Ag nanoparticles, if it is present, can be negligible or can only affect the amorphous regions of PEO fibers.

It is important to note that the main PEO lines corresponding to (120) and (112) reflections planes are broadened by the addition of Ag nanoparticles. The broadening is usually originated from the decrease of the crystallite size or by significant strains of the polymer chains due to the accommodation of the nanofiller. It is suggested that both contributions can affect the width of PEO diffraction lines.

### 3.5 | Raman spectroscopy analysis

The Raman spectra of PEO and PEO nanofibers loaded with various amounts of Ag NPs are shown in Figure 5. Significant differences between the Raman spectrum of the PEO powder and the Raman spectra of centrifugally spun PEO and PEO/Ag fibers are observed since metallic silver is not a Raman active material. However, oxidized silver may exhibit some Raman lines. Based on the X-ray data that have not revealed the presence of silver oxides, and the lack of Raman lines relevant to oxidized silver, it will be assumed that the Raman spectrum is controlled by Raman lines originated from the polymer matrix. Ag NPs are expected to exhibit surface-enhancing features as well as significant position's shifts due to the plasmon-mediated interaction between Ag NPs and the PEO macromolecular chains. Thus, some regions of the Raman spectrum may be preferentially enhanced. The centrifugally spun PEO and PEO/Ag nanofibers show significantly weaker lines compared to pristine PEO powder. It is important to note that the Raman lines of the PEO and PEO/Ag fibrous mats are wider

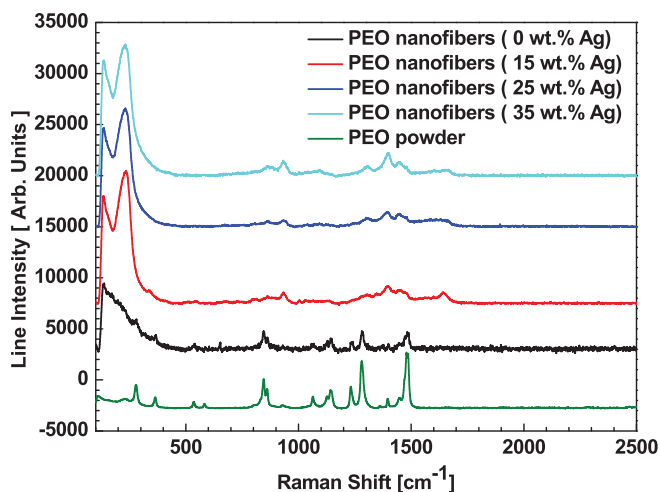


**FIGURE 5** Raman spectra of PEO and PEO-Ag nanocomposites

than those of the as-received PEO powder. The addition of Ag nanoparticles modified the PEO Raman spectrum and broadened the resonance lines, which was due to the interaction between Ag and the PEO-fiber matrix.

It is observed in Figure 5 that the Raman spectrum at low shifts (typically below  $500\text{ cm}^{-1}$ ) is enhanced by the addition of Ag NPs to the PEO-fiber matrix. The Raman shifts in the PEO/Ag composite nanofibers are assigned to (disorder) longitudinal acoustic modes (LAM), which is related to the elastic features of the polymer through the relationship<sup>65</sup>  $\tilde{\nu}_L \propto \sqrt{\frac{E}{\rho}}$ , where  $\tilde{\nu}_L$  defines the position of the Raman line,  $E$  is Young's modulus,  $\rho$  is the density,  $L$  is a length assigned to ordered regions of the polymer, and  $C$  is a constant. For disordered LAM modes,  $L$  is identified as the persistence length.<sup>65</sup> The line located at about  $120\text{ cm}^{-1}$  in the PEO-powder spectrum (Figure 6) and assigned to LAM was enhanced and shifted toward larger Raman shifts for the PEO/Ag composite fibers (up to about  $135\text{ cm}^{-1}$ ). Such increase of the Raman line suggests an increase of Young's modulus upon the addition of Ag nanoparticles. It is also possible that the order length,  $L$ , may be smaller in the centrifugally spun PEO and PEO/Ag nanofibers than that in the PEO powder. This may be understood by observing that the centrifugal forces favor the polymer crystallization for relatively low values. If the centrifugal forces were sufficiently high, then they would generate a local internal stress capable to break the crystallites that grow during centrifugal spinning.

The weak and broad line noticed in the PEO powder at about  $230\text{ cm}^{-1}$  is not significantly affected in the PEO fibrous mat but is enhanced by the loading with Ag nanoparticles. This amplification of the spectrum is not observed for all investigated wavenumbers suggesting a preferentially surface enhanced Raman scattering (SERS).

The Raman lines located at about  $280$  and  $360$ ,  $535\text{ cm}^{-1}$  in the PEO powder were also noticed in the PEO fibrous mat but disappeared after the Ag nanoparticles were added to the PEO-fiber

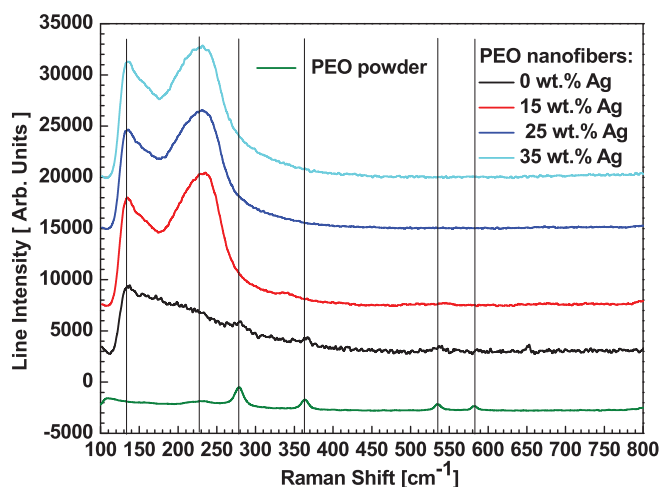


**FIGURE 6** Relationship between line intensity and Raman shift of PEO/Ag composite nanofibers with different concentrations. The Raman lines in the fingerprint region are broadened and shifted by the addition of Ag NP, making a difficult precise quantification of their parameters

matrix. The lines located at 280 and 360  $\text{cm}^{-1}$  were assigned to LAM mode.<sup>62,66</sup> These lines disappeared as the concentration of the nanofiller increased in the PEO fibers.<sup>62</sup> A similar behavior was observed as the Ag content was increased. These changes may reflect strong interactions between Ag NPs and the PEO macromolecular chains. Figure 6 shows that the Raman line located at 580  $\text{cm}^{-1}$  in PEO powder disappeared in all PEO mats (loaded or not with Ag nanoparticles).

### 3.6 | Antibacterial analysis

Antibacterial tests were conducted on the Gram-negative *E. coli* bacteria and Gram-positive *B. cereus* bacteria using PEO/Ag composite nanofibers as the antibacterial agent. The activity was performed using the disk diffusion method. Figure 7(A–F) shows the assessment of PEO/Ag (15, 25, and 35 wt%) composite nanofibrous membranes on the growth inhibition of those two bacteria.

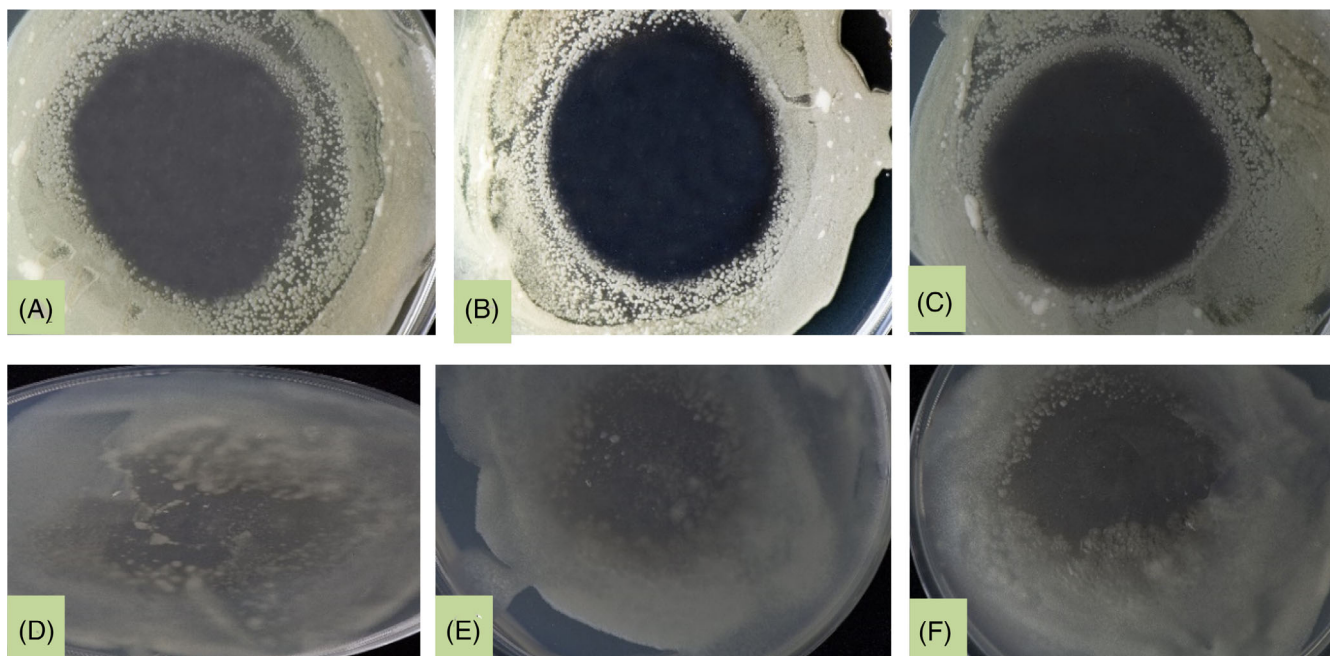
From Figure 7(A–C), it is evident that the inhibition capacity of membrane on *E. coli* is more than for *B. cereus* indicated as in Figure 7(D–F). After 24 h, *E. coli* was near about fully inhibited by the membrane, while *B. cereus* was less inhibited than *E. coli*. Therefore, the PEO/Ag nanofibrous membrane is more effective to impede Gram-negative bacterial strain. From the experimental data, it was observed that the inhibition zone growth in case of *E. coli* was 97%, 100%, and 100% for Ag concentration of 15, 25, and 35 wt%, respectively, in 24 h (Figure 7(A–C)) where the average inhibition diameter was 12.7 out of 12.7 mm. However, in the case of *B. cereus*, there were few portions on the fibrous membrane where the pathogenic

bacteria grew overtime. As indicated in Figure 7(D–F), inhibition capacity was 78%, 90%, and 95%, respectively, for the above three Ag concentrations. The standard deviations for the antimicrobial activity measurements of PEO/Ag composite fibers against *E. coli* and *S. aureus* are given in Table 1.

After 1-day performance test of PEO/Ag nanofibers on *B. cereus*, the zone of growth inhibition was calculated as an average of 11.1 mm out of the sample diameter (12.7 mm) (Figures 7(C, D)). This inhibition capacity was observed only because of the content of Ag nanoparticles embedded into the PEO nanofibers since pure PEO nanofibers did not have any antibacterial activity on bacteria. The interaction between silver ions and bacteria can spoil metabolic activity of bacteria through inactivating its cell which mechanism has been described in introduction.<sup>48–50</sup> Basically, Ag NPs dispersed outside the nanofibrous membrane dissociated to Ag + ion and were attracted to bacterial negative ion to dysfunction cells.<sup>11,49</sup> The results show that the 35% Ag-loading hollow fibers were the most efficient to inhibit the bacterial growth (Figure 8).

### 3.7 | In vitro release study

Figure 9 shows the dissolution of the pure Ag NPs exposed to ultra-pure water over a 1-week time period. As can be seen in Figure 9, the NPs are soluble within the first day (24 h), and then the solubility of silver was decreased by 72 h of exposure. Subsequently, the solubility of Ag nanoparticles was increased again by the fifth and seventh days of contact. The decrease in concentration observed at 72 h of reaction may have been due to the reprecipitation of the dissolved silver onto

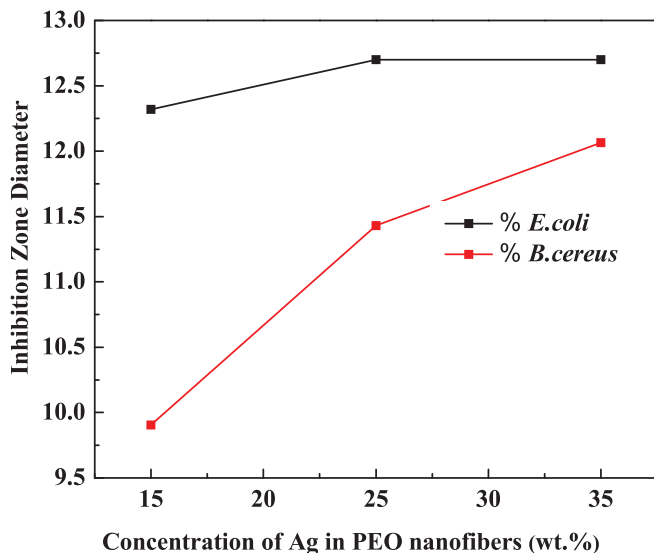
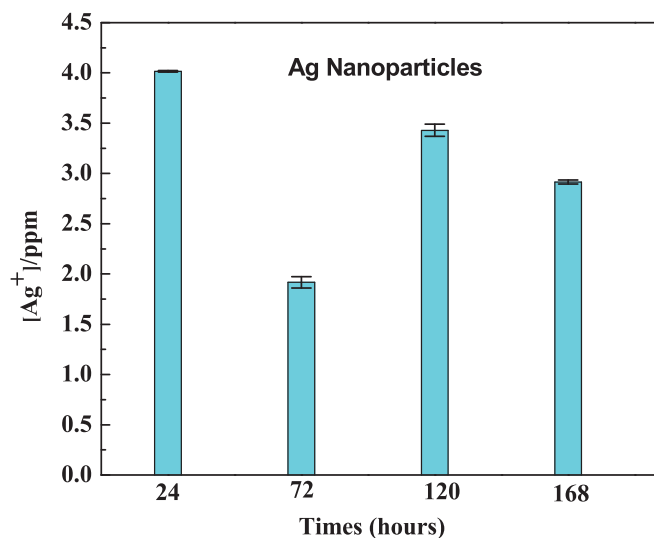


**FIGURE 7** Antimicrobial activity of nonwoven silver nanoparticles-embedded PEO composite membranes against *E. coli* (A–C) and against *B. cereus* (D–F)



**TABLE 1** Inhibition zone diameter for the antibacterial activity of PEO/Ag nanofibers

Fibers with bacteria	Average diameter of inhibition zone(mm)	Standard Deviation (mm)
PEO/Ag in <i>E. coli</i>	12.573 out of 12.7	0.2194
PEO/Ag in <i>B. cereus</i>	11.1337 out of 12.7	1.1096

**FIGURE 8** Relationship between Ag concentration and inhibition zone diameter (the nanofiber sample size was 12.7 mm)**FIGURE 9** Concentration of Ag<sup>+</sup> released for the Ag NPs sample as a function of the immersion time

the surface of the reaction tube. Figure 10 shows the dissolution of the 15 wt% Ag NPs in PEO nanofibers. As can be seen in Figure 10, the concentration of Ag in solution was observed to increase with time.

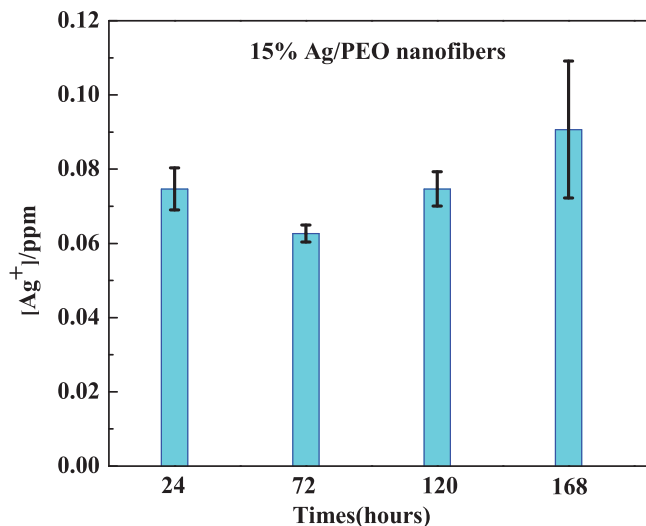
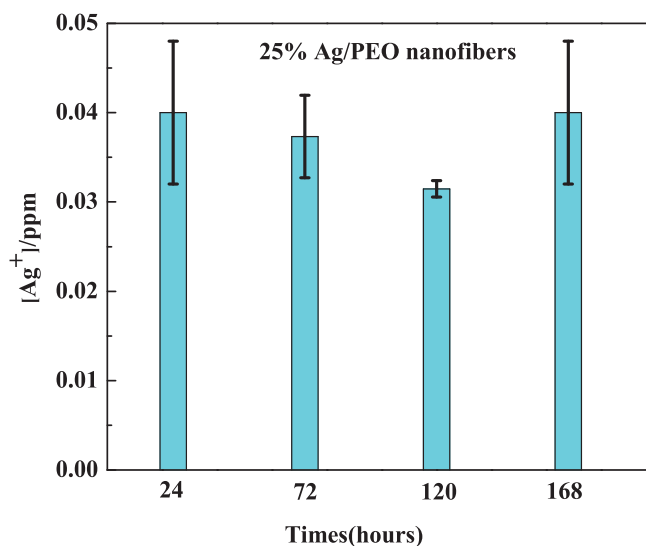
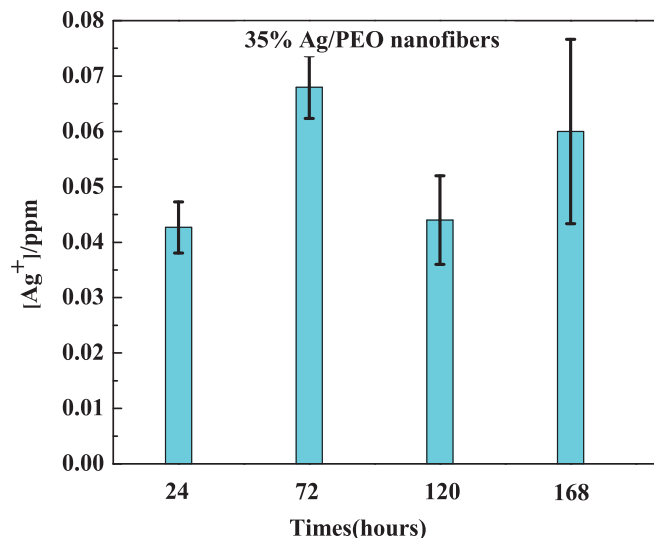
**FIGURE 10** Concentration of Ag<sup>+</sup> released for the 15% Ag/PEO composite nanofibers sample as a function of the immersion time**FIGURE 11** Concentration of Ag<sup>+</sup> released for the 25% Ag/PEO composite nanofibers sample as a function of the immersion time

Figure 11 shows the dissolution of the 25 wt% Ag NPs in PEO nanofibers. The results in Figure 11 show that the dissolution of the Ag from the PEO fiber matrix was relatively constant over the 5 days, meaning that the sample initially dissolved and the concentration of silver in the solution did not increase to any great extent. Figure 12 shows the dissolution of 35 wt% Ag in PEO nanofibers exposed to ultra-pure water for up to 1 week. As can be seen in Figure 12, the dissolution of the sample was relatively constant after the first 24 h. The data indicate that the dissolution of the Ag NPs and the Ag NPS in PEO nanofibers occurred primarily within the first 24 h and either increased slightly or remained relatively constant thereafter.



**FIGURE 12** Concentration of Ag<sup>+</sup> released for the 35% Ag/PEO composite nanofibers sample as a function of the immersion time

## 4 | CONCLUSIONS

PEO/Ag composite nanofibers, with an average diameter of 232.8 nm, were prepared from PEO/Ag precursor solutions through centrifugal spinning. The nanofibrous membranes were fabricated by optimizing the spinneret rotational speed at 5000 rpm, 8 wt% polymer concentration, and 43% relative humidity. The PEO/Ag composite fibers were in the form of thick fibrous mats in that the Ag nanoparticles were dispersed uniformly in the PEO-fiber matrix as the SEM, EDS, and Raman characterization proved except for a few agglomerated clusters. The antibacterial performance of the composite fibers showed impressive results. In agar plate, the inhibition zone was vividly seen where on average, the inhibition efficiency against *E. coli* and *B. cereus* bacteria was 99% and 88%, respectively. Such improved antimicrobial function of the PEO/Ag composite nanofibers was attributed to the porous structure with higher surface area because of which Ag NPs were embedded very spatially to impede the bacterial action effectively. The more the content of Ag<sup>+</sup> be embedded in an optimized range, the more the capacity the nanofibrous membrane to dysfunction the bacterial cell due to the negative ion of the membrane. Therefore, centrifugally spun Ag/PEO nanofibers might be a potential treatment for the prevention of the bacterial strains.

## ACKNOWLEDGEMENTS

This research was supported by the USDA, the National Institute of Food and Agriculture, and the Integrating Food Science/Engineering and Education Network (IFSEEN) with award number: 2015-38422-24059. This work was also supported by National Science Foundation (NSF) PREM award under grant no. DMR-1523577: UTRGV-UMN Partnership for Fostering Innovation by Bridging Excellence in Research and Student Success.

## DATA AVAILABILITY STATEMENT

The data that support the findings of this study are available from the corresponding author upon reasonable request.

## ORCID

Mataz Alcoutlabi  <https://orcid.org/0000-0003-4641-9109>

## REFERENCES

- Xu F, Weng B, Materon LA, Gilkerson R, Lozano K. Large-scale production of a ternary composite nanofiber membrane for wound dressing applications. *J Bioact Compat Polym*. 2014;29:646-660.
- Froon AH, Dentener MA, Greve JWM, Ramsay G, Buurman WA. Lipopolysaccharide toxicity-regulating proteins in bacteremia. *J Infect Dis*. 1995;171:1250-1257.
- Kieft H, Hoepelman AI, Zhou W, Rozenberg-Arska M, Struyvenberg A, Verhoef J. The sepsis syndrome in a Dutch university hospital: clinical observations. *Arch Intern Med*. 1993;153:2241-2247.
- Bolin MH, Svennersten K, Wang X, et al. Nano-fiber scaffold electrodes based on PEDOT for cell stimulation. *Sensors Actuators B Chem*. 2009;142:451-456.
- Lumley JL. Drag reduction by additives. *Annu Rev Fluid Mech*. 1969;1:367-384.
- Pham QP, Sharma U, Mikos AG. Electrospinning of polymeric nanofibers for tissue engineering applications: a review. *Tissue Eng*. 2006;12:1197-1211.
- Khanam N, Mikoryak C, Draper RK, Balkus KJ Jr. Electrospun linear polyethyleneimine scaffolds for cell growth. *Acta Biomater*. 2007;3:1050-1059.
- Kumbar S, James R, Nukavarapu S, Laurencin C. Electrospun nanofiber scaffolds: engineering soft tissues. *Biomed Mater*. 2008;3:034002.
- Min B-M, Lee G, Kim SH, Nam YS, Lee TS, Park WH. Electrospinning of silk fibroin nanofibers and its effect on the adhesion and spreading of normal human keratinocytes and fibroblasts in vitro. *Biomaterials*. 2004;25:1289-1297.
- Mattioli-Belmonte M, Zizzi A, Lucarini G, et al. Chitin nanofibrils linked to chitosan glycolate as spray, gel, and gauze preparations for wound repair. *J Bioact Compat Polym*. 2007;22:525-538.
- Xu F, Weng B, Materon LA, Kuang A, Trujillo JA, Lozano K. Fabrication of cellulose fine fiber based membranes embedded with silver nanoparticles via Forcespinning. *J Polym Eng*. 2016;36:269-278.
- Zhang XG, Qiao JX, Zhao H, et al. Preparation and performance of novel polyvinylpyrrolidone/polyethylene glycol phase change materials composite fibers by centrifugal spinning. *Chem Phys Lett*. 2018;691:314-318.
- Zhang ZM, Chen BY, Lai ZL, Wang JW, Duan YS. Spinning solution flow model in the nozzle and experimental study of nanofibers fabrication via high speed centrifugal spinning. *Polymer*. 2020;205:122794.
- Zuniga L, Gonzalez G, Chavez RO, Myers JC, Lodge TP, Alcoutlabi M. Centrifugally spun alpha-Fe2O3/TiO2/carbon composite fibers as anode materials for lithium-ion batteries. *Appl Sci-Basel*. 2019;9:4032.
- Li D, Xia Y. Electrospinning of nanofibers: reinventing the wheel? *Adv Mater*. 2004;16:1151-1170.
- Paneva D, Bougard F, Manolova N, Dubois P, Rashkov I. Novel electrospun poly (ε-caprolactone)-based bicomponent nanofibers possessing surface enriched in tertiary amino groups. *Eur Polym J*. 2008;44:566-578.
- Ramakrishna S, Fujihara K, Teo WE, Lim TC, Ma Z. Introduction to Electrospinning and Nanofibers, World Scientific 2005:1-383.
- Saiyasombat C, Maensiri S. Fabrication, morphology, and structure of electrospun PAN-based carbon nanofibers. *J Polym Eng*. 2008;28:5-18.

19. De la Garza D, De Santiago F, Materon L, Chipara M, Alcoutlabi M. Fabrication and characterization of centrifugally spun poly(acrylic acid) nanofibers. *J Appl Polym Sci*. 2019;136:47480.
20. Weng BC, Xu FH, Garza G, Alcoutlabi M, Salinas A, Lozano K. The production of carbon nanotube reinforced poly(vinyl) Butyral nanofibers by the Forcespinning (R) method. *Polym Eng Sci*. 2015;55:81-87.
21. Agubra VA, De la Garza D, Gallegos L, Alcoutlabi M. ForceSpinning of polyacrylonitrile for mass production of lithium-ion battery separators. *J Appl Polym Sci*. 2016;133:42847.
22. Zander NE. Formation of melt and solution spun Polycaprolactone fibers by centrifugal spinning. *J Appl Polym Sci*. 2015;132:41269.
23. Chen G, Shi TT, Zhang XG, et al. Polyacrylonitrile/polyethylene glycol phase-change material fibres prepared with hybrid polymer blends and nano-SiC fillers via centrifugal spinning. *Polymer*. 2020;186:122012.
24. Wang Y, Li M, Rong J, et al. Enhanced orientation of PEO polymer chains induced by nanoclays in electrospun PEO/clay composite nanofibers. *Colloid Polym Sci*. 2013;291:1541-1546.
25. Nista SVG, Bettini J, Mei LHI. Coaxial nanofibers of chitosan-alginate-PEO polycomplex obtained by electrospinning. *Carbohydr Polym*. 2015;127:222-228.
26. Kim J, Lee J, Kwon S, Jeong S. Preparation of biodegradable polymer/silver nanoparticles composite and its antibacterial efficacy. *J Nanosci Nanotechnol*. 2009;9:1098-1102.
27. Nair S, Natarajan S, Kim SH. Fabrication of electrically conducting polypyrrole-poly (ethylene oxide) composite nanofibers. *Macromol Rapid Commun*. 2005;26:1599-1603.
28. Ma G, Fang D, Liu Y, Zhu X, Nie J. Electrospun sodium alginate/poly (ethylene oxide) core-shell nanofibers scaffolds potential for tissue engineering applications. *Carbohydr Polym*. 2012;87:737-743.
29. Savaş H, Güven O. Investigation of active substance release from poly (ethylene oxide) hydrogels. *Int J Pharm*. 2001;224:151-158.
30. Desai NP, Hubbell JA. Biological responses to polyethylene oxide modified polyethylene terephthalate surfaces. *J Biomed Mater Res*. 1991;25:829-843.
31. Nagaoka S, Nakao A. Clinical application of antithrombogenic hydrogel with long poly (ethylene oxide) chains. *Biomaterials*. 1990;11:119-121.
32. Kim S, Kim JH, Kim JO, Ku S, Cho H, Huh P. Fabrication of poly (ethylene oxide) hydrogels for wound dressing application using E-beam. *Macromol Res*. 2014;22:131-138.
33. Thirugnanaselvam M, Gobi N, Arun Karthick S. SPI/PEO blended electrospun matrix for wound healing. *Fibers Polym*. 2013;14:965-969.
34. Kohsari I, Shariatnia Z, Pourmortazavi SM. Antibacterial electrospun chitosan-polyethylene oxide nanocomposite mats containing bioactive silver nanoparticles. *Carbohydr Polym*. 2016;140:287-298.
35. Selvam S, Sundrarajan M. Functionalization of cotton fabric with PVP/ZnO nanoparticles for improved reactive dyeability and antibacterial activity. *Carbohydr Polym*. 2012;87:1419-1424.
36. Alhusiki-Alghamdi HM, Alghunaim NS. Spectroscopic studies of nanocomposites based on PEO/PVDF blend loaded by SWCNTs. *J Mod Phys*. 2015;6:414-424.
37. Avci H, Monticello R, Kotek R. Preparation of antibacterial PVA and PEO nanofibers containing *Lawsonia inermis* (henna) leaf extracts. *J Biomater Sci Polym Ed*. 2013;24:1815-1830.
38. Cheah WY, Show P-L, Ng IS, Lin G-Y, Chiu C-Y, Chang Y-K. Antibacterial activity of quaternized chitosan modified nanofiber membrane. *Int J Biol Macromol*. 2019;126:569-577.
39. Marini M, Bondi M, Iseppi R, Toselli M, Pilati F. Preparation and antibacterial activity of hybrid materials containing quaternary ammonium salts via sol-gel process. *Eur Polym J*. 2007;43:3621-3628.
40. Mahltig B, Gutmann E, Meyer DC, et al. Solvothermal preparation of metallized titania sols for photocatalytic and antimicrobial coatings. *J Mater Chem*. 2007;17:2367-2374.
41. Malwal D, Gopinath P. Efficient adsorption and antibacterial properties of electrospun CuO-ZnO composite nanofibers for water remediation. *J Hazard Mater*. 2017;321:611-621.
42. Shamel K, Ahmad MB, Jazayeri SD, et al. Investigation of antibacterial properties silver nanoparticles prepared via green method. *Chem Cent J*. 2012;6:73.
43. Yalcinkaya F, Lubasova D. Quantitative evaluation of antibacterial activities of nanoparticles (ZnO, TiO<sub>2</sub>, ZnO/TiO<sub>2</sub>, SnO<sub>2</sub>, CuO, ZrO<sub>2</sub>, and AgNO<sub>3</sub>) incorporated into polyvinyl butyral nanofibers. *Polym Adv Technol*. 2017;28:137-140.
44. Sadeghi B, Jamali M, Kia S, Nia AAMINI, Ghafari S. Synthesis and characterization of SILVER nanoparticles for antibacterial activity. *Int J Nano Dimens (IJND)*. 2010;1:119-124.
45. Sarwar MS, Niazi MBK, Jahan Z, Ahmad T, Hussain A. Preparation and characterization of PVA/nanocellulose/ag nanocomposite films for antimicrobial food packaging. *Carbohydr Polym*. 2018;184:453-464.
46. Quirós J, Borges JP, Boltes K, Rodea-Palomares I, Rosal R. Antimicrobial electrospun silver-, copper- and zinc-doped polyvinylpyrrolidone nanofibers. *J Hazard Mater*. 2015;299:298-305.
47. Basri H, Ismail AF, Aziz M. Polyethersulfone (PES)-silver composite UF membrane: effect of silver loading and PVP molecular weight on membrane morphology and antibacterial activity. *Desalination*. 2011;273:72-80.
48. van der Wal A, Norde W, Zehnder AJB, Lyklema J. Determination of the total charge in the cell walls of gram-positive bacteria. *Colloids Surf B Biointerfaces*. 1997;9:81-100.
49. Guzman M, Dille J, Godet S. Synthesis and antibacterial activity of silver nanoparticles against gram-positive and gram-negative bacteria. *Nanomedicine*. 2012;8:37-45.
50. Su H-L, Chou C-C, Hung D-J, et al. The disruption of bacterial membrane integrity through ROS generation induced by nanohybrids of silver and clay. *Biomaterials*. 2009;30:5979-5987.
51. Zupančič S, Rijavec T, Lapanje A, Petelin M, Kristl J, Kocbek PJB. Nanofibers with incorporated autochthonous bacteria as potential probiotics for local treatment of periodontal disease. *Bio-macromolecules*. 2018;19:4299-4306.
52. Sarkar K, Gomez C, Zambrano S, et al. Electrospinning to forcespinning™. *Mater Today*. 2010;13:12-14.
53. Agubra VA, Zuniga L, De la Garza D, Gallegos L, Pokhrel M, Alcoutlabi M. Forcespinning: a new method for the mass production of Sn/C composite nanofiber anodes for lithium ion batteries. *Solid State Ionics*. 2016;286:72-82.
54. Agubra VA, Zuniga L, Flores D, Campos H, Villarreal J, Alcoutlabi M. A comparative study on the performance of binary SnO<sub>2</sub>/NiO/C and Sn/C composite nanofibers as alternative anode materials for lithium ion batteries. *Electrochim Acta*. 2017;224:608-621.
55. Jorge Lopez RG, Ayala J, Cantu J, et al. Centrifugally spun TiO<sub>2</sub>/C composite fibers prepared from TIS2/PAN precursor fibers as binder-free anodes for LIBS. *J Phys Chem Solids*. 2021;149:109795.
56. Flores D, Villarreal J, Lopez J, Alcoutlabi M. Production of carbon fibers through forcespinning (R) for use as anode materials in sodium ion batteries. *Mater Sci Eng B-Adv*. 2018;236:70-75.
57. Kizildag N, Ucar N. Investigation of the properties of PAN/f-MWCNTs/AgNPs composite nanofibers. *J Ind Text*. 2017;47:149-172.
58. Chavez RO, Lodge TP, Alcoutlabi MJMS. Recent developments in centrifugally spun composite fibers and their performance as anode materials for lithium-ion and sodium-ion batteries. *Materials Science and Engineering*. 2021;266:115024.
59. Lin JY, Ding B, Yu JY, Hsieh Y. Direct fabrication of highly Nanoporous polystyrene fibers via electrospinning. *ACS Appl Mater Interfaces*. 2010;2:521-528.
60. Tong Y, Lin Y, Wang S, Song M. A study of crystallisation of poly (ethylene oxide) and polypropylene on graphene surface. *Polymer*. 2015;73:52-61.

61. Wang W, Alexandridis P. Composite polymer electrolytes: nanoparticles affect structure and properties. *Polymer*. 2016;8:387.
62. Chipara DM, Panaitescu DM, Lozano K, Gabor RA, Nicolae CA, Chipara M. Raman spectroscopy and molecular bases of elasticity: SEBS-graphite composites. *Polymer*. 2019;176:74-88.
63. Shameli K, Ahmad MB, Zamanian A, et al. Green biosynthesis of silver nanoparticles using *Curcuma longa* tuber powder. *Int J Nanomedicine*. 2012;7:5603-5610.
64. Liu S, Huang W, Chen S, Avivi S, Gedanken A. Synthesis of X-ray amorphous silver nanoparticles by the pulse sonoelectrochemical method. *J Non-Cryst Solids*. 2001;283:231-236.
65. Migliardo F, Magazù S, Caccamo MT. Infrared, Raman and INS studies of poly-ethylene oxide oligomers. *J Mol Struct*. 2013;1048:261-266.
66. Chipara D, Kuncser V, Lozano K, Alcoutlabi M, Ibrahim E, Chipara M. Spectroscopic investigations on PVDF-Fe<sub>2</sub>O<sub>3</sub> nanocomposites. *J Appl Polym Sci*. 2020;137:48907

**How to cite this article:** Hasan MT, Gonzalez R, Chipara M, Materon L, Parsons J, Alcoutlabi M. Antibacterial activities of centrifugally spun polyethylene oxide/silver composite nanofibers. *Polym Adv Technol*. 2021;1-12. <https://doi.org/10.1002/pat.5261>